East European Journal of Physics. 2. 88–100 (2026)
DOI: 10.26565/2312-4334-2026-2-08 ISSN 2312-4334

DOPPLER SPECTRA FOR STATIONARY AND DYNAMIC ULTRASONIC FIELDS

Evgen A. Barannik, **Mykhailo O. Hrytsenko***
Department of Medical Physics and Biomedical Nanotechnologies, V.N. Karazin Kharkiv National University
4 Svobody Sq., 61022, Kharkiv, Ukraine
**Corresponding Author e-mail: mykhailo.hrytsenko@student.karazin.ua*
Received February 25, 2026; revised April 12, 2026; accepted May 3, 2026

This paper presents a review of physical and methodological approaches to describing the spectrum of the ultrasonic Doppler signal in biological media. The results on the formation of spectral characteristics for a stationary probing field under different types of scatterer motion are summarized, and the development of the model for the case of a dynamically varying sensitivity function of the ultrasound system is considered. Particular attention is paid to synthetic aperture, dynamic focusing, and coherent plane-wave compounding modes. It is shown that in plane-wave imaging systems the Doppler signal spectrum is determined not only by the motion properties of the medium, but also by the spatiotemporal method used to form the Doppler response. The results concerning spatial resolution in the plane-wave compounding mode are also summarized, and the relationship between the geometry of the measurement volume, the sensitivity function, and the spectral parameters is analyzed. Prospects for the further development of these approaches, in particular for applications in shear-wave elastography, are outlined.

Keywords: *Ultrasound Doppler imaging; Doppler spectrum; Synthetic aperture imaging; Plane-wave imaging; Coherent plane-wave compounding; Spatial resolution; Shear-wave elastography*

PACS: 43.28.Py, 43.35.Yb, 43.60.-c, 87.63.D-, 87.63.dk

1. INTRODUCTION

Ultrasound blood-flow imaging is currently undergoing a period of rapid methodological transformation, evolving from conventional Doppler modes toward high-frame-rate, microvascular, and volumetric approaches capable of visualizing slow flow and fine vascular architecture much better than conventional color or power Doppler [1–5]. This evolution is driven by the fundamental limitations of traditional line-by-line scanning, which inherently involves trade-offs among frame rate, contrast, spatial resolution, and sensitivity to low-velocity flow. In addition, conventional two-dimensional ultrasound imaging strongly depends on the imaging plane and operator experience, whereas modern volumetric and ultrafast approaches provide broader opportunities for functional and vascular imaging [1, 2, 4].

The theoretical foundation of this transition was established by synthetic aperture imaging and coherent plane-wave compounding (CPWC), which introduced a fundamentally different image formation strategy compared with sequential focused transmission [6, 7]. These studies laid the groundwork for ultrasound imaging with very high frame rates, transient elastography, and the further development of ultrafast Doppler methods. At the same time, the plane-wave approach proved promising not only for B-mode and Doppler applications, but also for contrast-enhanced imaging, where it can be competitive with focused transmission [8].

The current development of this field is taking place along several interconnected directions. First, the basic image-formation algorithms are being actively improved: synthetic focusing schemes are being optimized, and new approaches based on reverse time migration, minimum-variance adaptive beamforming, high-contrast compounding, as well as software environments for fast and reproducible simulation of plane-wave and color Doppler imaging are being developed [9–13]. Second, considerable attention is being paid to the computational feasibility of such methods, including GPU implementations of synthetic aperture approaches and hybrid transmission schemes that improve spatiotemporal resolution in problems involving rapid motion, particularly in echocardiography [14, 15]. Third, ongoing work seeks an optimal balance between image quality and frame rate. To this end, researchers employ adaptive beamforming for multi-angle plane-wave imaging, null-subtraction imaging schemes, aperture extension using multiple arrays, adaptive combining, tensor completion, and other accelerated CPWC approaches [16–21]. For Doppler and microvascular imaging modes, specialized beamforming schemes are also being developed, including retrospective transmit beamforming, DMAS, and computationally efficient nonlinear compounding methods [22–24]. Particular note should also be made of the growing role of artificial intelligence and deep learning, which are used not only for post-processing but also for compensating the fundamental limitations of single-plane-wave imaging and accelerated compounding [25, 26].

The clinical significance of these technologies already extends far beyond purely technical demonstrations. Ultrafast and microvascular ultrasound methods are being applied to assess muscle perfusion, detect synovitis at an early stage, screen for renal artery disease, and noninvasively evaluate myocardial perfusion [27–30]. In thyroid diagnostics, microvascular imaging improves the accuracy of nodule risk stratification and complements standard grayscale ultrasound examination

Cite as: E.A. Barannik, M.O. Hrytsenko, East Eur. J. Phys. 2, 88 (2026), https://doi.org/10.26565/2312-4334-2026-2-08

[31–33]. In oncology, these approaches, including super-resolution ultrasound imaging, open new possibilities for more accurate lesion differentiation, preoperative staging, assessment of microvascular architecture, and early monitoring of treatment response [34–38].

The present review focuses on the sequential development of physical and methodological approaches to ultrasound and Doppler image formation in synthetic aperture and plane-wave compounding systems—from the analysis of the spectrum of individual flow lines for focused transducers with apodization in the early 2000s to the construction of a continuous scattering model, its extension to the case of a dynamically varying sensitivity function, the study of spectra under changing insonification angles, and the evaluation of spatial resolution, point spread function, and measurement-volume shape in plane-wave compounding modes in studies published in 2022–2025. This temporal perspective, covering the development of the topic from 2001 to the present, makes it possible to trace how the basic concepts of the Doppler spectrum, sensitivity function, and measurement-volume geometry became the foundation for modern high-speed and full-field methods of blood-flow imaging and parameter estimation.

2. PHYSICAL MODEL

In [39], the spectrum of the Doppler signal from an individual flow line in the pulsed mode was studied for focused transducers with apodized apertures. It was shown that the spectral characteristics are determined not only by the velocity of scatterer motion, but also by the parameters of the ultrasound field itself. The intrinsic spectral broadening is caused by two factors: the finite residence time of scatterers within the measurement volume and the curvature of the wavefronts, which changes the local Doppler angle. For a fixed depth, the width of the spectrum of an individual flow line does not depend on its position within the measurement volume, but it changes with the insonification depth. By contrast, the modal Doppler shift depends on both the depth and the position of the flow line if the center of the measurement volume does not coincide with the focus. Thus, already in this work, the Doppler spectrum appears as the result of the combined action of flow kinematics and the geometry of the ultrasound field.

In all subsequent papers, the main physical hypothesis remains the same: the biological medium is treated as isotropic and continuous, and ultrasound is scattered by small fluctuations of density $\rho(\vec{r},t)$ and compressibility $\beta(\vec{r},t)$. The smallness of these fluctuations makes it possible to restrict the analysis to single scattering, and then the response of the pulsed Doppler signal from the region of interest R can be written as [40, 41]

$$f = k^2 \int\limits_R e^{2i(\vec{k}\cdot\vec{r}+\theta_c)} C'_p \left[\tilde{\beta}(\vec{r},t) - \tilde{\rho}(\vec{r},t)\gamma(\vec{r},t)\right] d^3\vec{r}. \tag{1}$$

Here, $\vec{k}$ and $k = 2\pi/\lambda$ are the wave vector and the wave number in the plane-wave approximation for an ultrasound wavelength λ propagating with velocity c. θ_c is the constant phase component of the signal, $\tilde{\rho}(\vec{r},t) = [\rho(\vec{r},t) - \rho_0]\rho_0^{-1} \ll 1$ and $\tilde{\beta}(\vec{r},t) = [\beta(\vec{r},t) - \beta_0]\beta_0^{-1} \ll 1$ are the dimensionless density and compressibility functions, while ρ_0 and β_0 are the spatiotemporal mean values of the density and compressibility of the medium, respectively. The quantity $\gamma(\vec{r},t) \cong 1$ is a dimensionless parameter characterizing the deviation of the wavefront shape from that of ideal plane waves.

The Doppler response can be defined through the complex sensitivity functions (amplitudes) of the transmitted field $G'_t(\vec{r})$, the receiver sensitivity to the scattered waves $G'_r(\vec{r})$, and $b(t)$, the envelope of the probing pulse. Here, $x'(\vec{r})$ is the distance from the point $\vec{r}$ along the probing axis, and T_1 is the delay time determining the ultrasound depth:

$$G'_p(\vec{r}) = G_t(\vec{r})\, G_r(\vec{r})\, b\left(T_1 - \frac{2x'(\vec{r})}{c}\right). \tag{2}$$

The spatiotemporal correlator of the inhomogeneities is

$$C(\vec{r}_1 - \vec{r}_0, \tau) = \left\langle \left(\tilde{\beta}(\vec{r}_0,t_0) - \tilde{\rho}(\vec{r}_0,t_0)\right)\left(\tilde{\beta}(\vec{r}_1,t_1) - \tilde{\rho}(\vec{r}_1,t_1)\right)\right\rangle. \tag{3}$$

It is expressed as an ensemble average and depends only on the time difference $\tau = t_1 - t_0$. Formally, this expression describes a dynamic medium: if C varies slowly as τ increases, then the echo will decorrelate slowly and the Doppler spectrum will be narrower than in the case of rapid variation. This function can be represented as a Fourier integral in the form of a sum of contributions from plane spatial harmonics:

$$C(\vec{r}_1 - \vec{r}_0, \tau) = \int \frac{d^3\vec{q}}{(2\pi)^3}\, e^{i\vec{q}\cdot(\vec{r}_1-\vec{r}_0)} \int \frac{d\omega}{2\pi}\, e^{-i\omega\tau}\, C(\vec{q},\omega). \tag{4}$$

Here, $C(\vec{q},\omega)$ is the power spectral density of the fluctuations, which indicates which spatial scales $\vec{q}$ of the inhomogeneities are associated with which temporal frequencies ω in the dynamics of the inhomogeneities. This representation makes it possible to separate the "physics of the object" from the "physics of the measurement": the correlator describes the structure and motion of the inhomogeneities, whereas the sensitivity function describes the geometry, focusing, pulse duration, and the transmission–reception configuration.

The nature of the fluctuations makes it possible to represent the Doppler response through the product of two entities: the correlator of medium fluctuations and the sensitivity function of the probing system. Within this continuous model, general expressions for the spectra were obtained for several fundamentally important cases, which will be discussed below. In this form, the model immediately separates the "physics of the object" from the "physics of the measurement": the correlator is responsible for the structure and dynamics of the inhomogeneities, whereas the sensitivity function is responsible for the field geometry, focusing, pulse duration, and the transmission–reception configuration. This approach forms the core of [41], [42], [43], and [44], and it is retained in [45, 46], where only the method of field representation is modified for plane-wave compounding.

Thus, the first significant generalization of the model was carried out in [42], where the stationary sensitivity function was replaced by a time-dependent one:

$$G'_p(\vec{r},t) = G_t(\vec{r})\, G_r(\vec{r},t)\, b\left(T_1 - \frac{2x'(\vec{r})}{c}\right). \tag{5}$$

This is the general form of the sensitivity function in the case of synthetic aperture, regardless of the method used to determine the Doppler shift frequency. Physically, this means that in synthetic aperture systems with dynamic variation of the insonification direction, not only the motion of the scatterers changes, but also the measurement scheme itself. In this case, the full power spectrum of the Doppler signal is related not only to the spectral characteristics of the motion of the inhomogeneities, but also to the spatial and temporal harmonics of the probing field. In the case of probing a biological medium by plane waves with different angles and wave vector $\vec{k}(t)$, as shown in Fig. 1, the envelope in (5) takes the form [43].

$$b(t) = b\left(T_1 - \frac{2x' \cos\Phi(t)}{c_0}\right). \tag{6}$$

In this case, the complex amplitude of the incident plane waves is taken with account of their deviation from the untilted plane wave, while $c_0/\cos\Phi(t)$ is the propagation velocity along the x' axis of the incident plane-wave front with wave-vector deviation angle $\Phi(t)$.

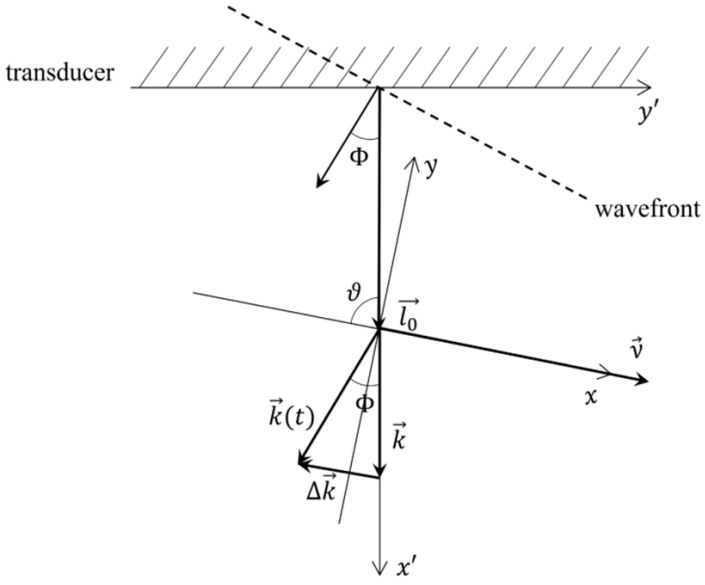

Figure 1. Arrangement of the unprimed coordinate system associated with the measurement volume relative to the ultrasound transducer, and the deviation angle of the wave vector $\vec{k}(t)$ of the current wave from the wave vector $\vec{k}$ of the untilted wave.

In [46], an approach based on the direct use of the transmitted wave field $P'_t(\vec{r},t)$ and the received wave field $P'_r(\vec{r},t)$, represented in the form of plane waves, was considered. In this case, the combined transmit–receive field can be written as

$$P(\vec{r},t) = P_0 e^{2i\vec{k}(t)\cdot\vec{r}}\, b\left(T_1 - \frac{2x''}{c_0}\right) g(z). \tag{7}$$

Here, P_0 is the field amplitude, $g(z)$ is the distribution along the z axis, and $b\left(T_1 - \frac{2x''}{c_0}\right)$ is the pulse envelope describing their spatial length in the $x'' = x''(x', y')$ direction, that is, in the direction of transmission and reception of plane waves for a given vector $\vec{k}(t)$ and the corresponding angle Φ (see Fig. 2).

In [44] and [46], the spatial properties of the Doppler response in the coherent plane-wave compounding mode were described through the system sensitivity function and the geometry of the measurement volume. In [44], it was shown that for a rectangular weighting window the sensitivity function takes a sinc-like form

$$G'_p(\vec{r}, \omega_j = 0) \cong G_0 \, \frac{\sin(k\Omega t y')}{k\Omega t y'} \, b\left(T_1 - \frac{2x'(\vec{r})}{c}\right). \tag{8}$$

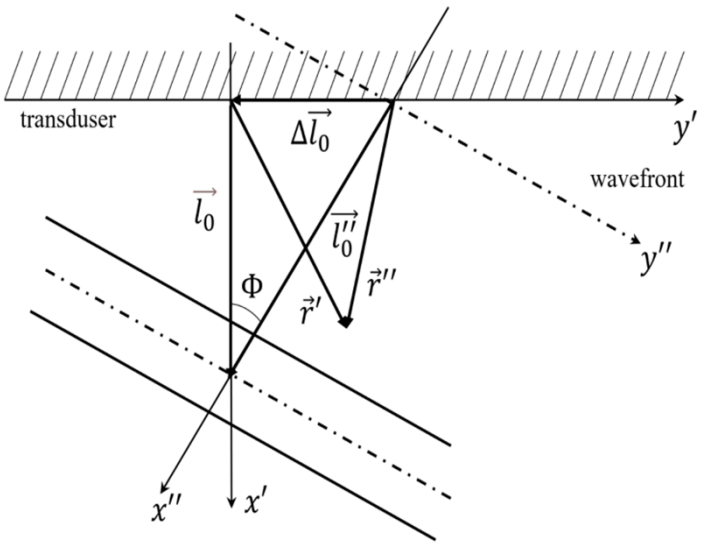

Figure 2. Coordinate system (x', y') associated with the ultrasound transducer, and coordinate system (x'', y'') in which the x'' axis is directed along the propagation direction of the plane-wave front.

therefore, the lateral resolution is determined primarily by the width of the angular insonification sector. In [46], this description was refined by taking into account small linear and quadratic angular terms in the envelope, which lead to a deformation of the boundary of the measurement volume, without changing the principal resolution scales along the coordinate axes. Thus, in the case of coherent plane-wave compounding, spatial selectivity is determined not only by the interference of responses from different viewing angles, but also by the geometry of their overlap region.

3. SPECTRUM OF THE DOPPLER RESPONSE IN THE CASE OF A STATIONARY PROBING FIELD

In most conventional pulsed systems, pulses are transmitted sequentially, with all of them characterized by the same geometry and configuration in the space of wavefronts. This means that the amplitude function of the transmitted field $G'_t(\vec{r})$ and the receiver sensitivity to the scattered waves $G'_r(\vec{r})$ do not depend on time, while the angle $\Phi = 0$. In this case, the Doppler spectrum can be obtained for stationary probing fields using either a single ultrasound emitter or a phased array that provides sequential transmission and reception of the reflected waves. The entire sequence is therefore characterized by one and the same wavefront geometry. In [41], a general expression was obtained for the power spectrum of the Doppler signal in the case of a stationary probing field:

$$S(\omega) = \frac{k^4}{(2\pi)^3} \int d\vec{q}\, C(\vec{q}, \omega) \left| G(\vec{q} + 2\vec{k}) \right|^2. \tag{9}$$

This is the most general relation between the power spectra of Doppler signals, the spectral characteristics of the fluctuations, and the parameters of the probing ultrasound field for a correlation volume small compared with the measurement volume. The factor $C(\vec{q}, \omega)$ describes the properties of the medium and its motion, that is, the structure and dynamics of the fluctuations, whereas $\left|G(\vec{q} + 2\vec{k})\right|^2$ acts as the spatial filter of the system, determined by the measurement volume and focusing. The measured Doppler spectrum is therefore their weighted combination. The authors emphasized that $G(\vec{q} + 2\vec{k})$ is a function with a sharp maximum at $\vec{q} = -2\vec{k}$, independently of the particular configuration of the ultrasound field in space and the way in which this field is described.

Based on the above, for stationary motion with a constant velocity $\vec{V}$ (for example, steady venous blood flow) and in the absence of diffusion, the authors isolated the power spectrum of individual Doppler flow lines using (9):

$$S_\nu(\omega, x, z) = k^4 \nu V \left\langle (\tilde{\beta} - \tilde{\rho})^2 \right\rangle \left| TF\left[e^{2ikV\cos\vartheta\, t}\, G'(Vt, y, z)\, b\left(T_1 - \frac{2x'(Vt, y, z)}{c}\right)\right]\right|^2. \tag{10}$$

Here, $TF[f(t)]$ denotes the Fourier transform of the function $f(t)$, ϑ is the Doppler angle between the transducer and the Ox axis, ν is the correlation volume, and in the analysis it was assumed that the motion occurs along the axis $x = Vt$ (Fig. 3). It was emphasized that the full spectrum is then the sum of the contributions from individual flow lines, while its shape is determined by the Doppler shift, the geometry of the measurement volume, and the spatial configuration of the ultrasound field. This case serves as the basic one for the further analysis of other physical factors.

The influence of spatial correlation of the inhomogeneities was considered separately. If a finite correlation radius Δ is introduced, then the contributions from different regions of the cross-section are no longer independent, and it becomes impossible to isolate the spectrum of individual flow lines. To estimate this effect, the authors used a Gaussian model of the sensitivity function, which made it possible to obtain an analytical expression for the spectrum:

$$S(\omega) = \frac{\pi^2 k^4 \nu \left\langle (\tilde{\beta} - \tilde{\rho})^2 \right\rangle}{8V} \frac{b^6}{2\Delta^2 + b^2} \exp\left\{ -\frac{1}{2\sigma^2} \left(\frac{\omega}{\omega_{md}} - 1 \right)^2 - \frac{\sigma^2 - \sigma_0^2}{2\sigma^2 \sigma_0^2 \cos^2 \vartheta} \right\}. \tag{11}$$

Here,

$$\omega_{md} = \omega_d \left(1 + \frac{2\Delta^2}{b^2} \right)^{-1}, \qquad \sigma^2 = \sigma_0^2 \left(1 + \frac{2\Delta^2}{b^2} \right).$$

The quantity ω_{md} is the modal Doppler frequency, which does not coincide with the conventional Doppler shift $\omega_d = -2kV \cos\vartheta$, while σ^2 is the dimensionless variance of the Doppler spectrum and σ_0^2 is the variance at $\Delta = 0$. Furthermore, $\nu = \alpha\Delta^3$ is the characteristic correlation volume, with α being a constant of order unity. Thus, spectral broadening may be caused not only by a distribution of velocities, but also by the correlation properties of the scatterers or of the motion itself. For this reason, in turbulent flow an increase in the power of the ultrasound and Doppler signals is not necessarily associated with erythrocyte aggregation or with changes in the density and compressibility of the medium; it may instead reflect correlated velocity pulsations.

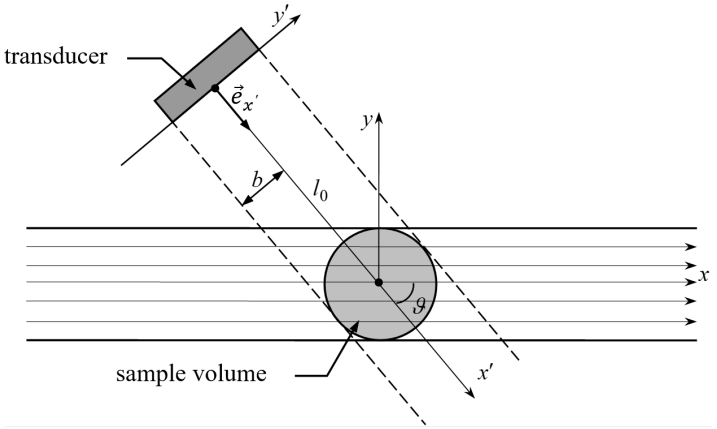

Figure 3. Schematic of the relative arrangement of the ultrasound transducer, the measurement volume, and the blood vessel. The Cartesian coordinate systems associated with the vessel (x, y, z) and with the ultrasound system (x_0, y_0, z_0) are shown, where l_0 is the insonification depth, θ is the Doppler angle, and b is the effective radius of the ultrasound beam at the e^{-1} level.

Another important factor is the diffusion of scatterers. To take it into account, the correlation function is written in a form satisfying the diffusion equation, and the corresponding spectrum takes the form

$$S(\omega) = \frac{k^4 \nu \left\langle (\tilde{\beta} - \tilde{\rho})^2 \right\rangle}{V} \int \frac{d^3\vec{q}}{(2\pi)^3} \frac{Dq^2}{(\omega - q_x V)^2 + (Dq^2)^2} \left| G(\vec{q} + 2\vec{k}) \right|^2. \tag{12}$$

Here, D is the diffusion coefficient. In this case, as in the case of a finite correlation radius, the contributions from individual flow lines can no longer be separated. It was shown that in the weak-diffusion limit this expression reduces to the spectrum for nondiffusive motion, whereas in the strong-mixing regime

$$V \ll 2bDk^2 \tag{13}$$

the spectrum becomes Lorentzian:

$$S(\omega) = \pi^{3/2} b^3 k^4 \nu \left\langle (\tilde{\beta} - \tilde{\rho})^2 \right\rangle \frac{Dk^2}{(\omega + 2kV\cos\vartheta)^2 + 16D^2k^4}. \tag{14}$$

Here, b is the parameter of the Gaussian sensitivity function characterizing the effective width of the incident and received ultrasound beams. Figure 4 shows the resulting normalized Doppler spectrum for the nondiffusive case and for cases with nonzero diffusion. For biological molecules, one typically has $D \sim 10^{-11}$–$10^{-10}\,\mathrm{m}^2/\mathrm{s}$; therefore, in blood vessels at ultrasound frequencies $f \approx 2$–$10\,\mathrm{MHz}$, diffusion is often weak and its influence on the spectra is usually neglected unless D becomes comparable to the critical value $D_{\mathrm{critical}} = V/(2bk^2)$.

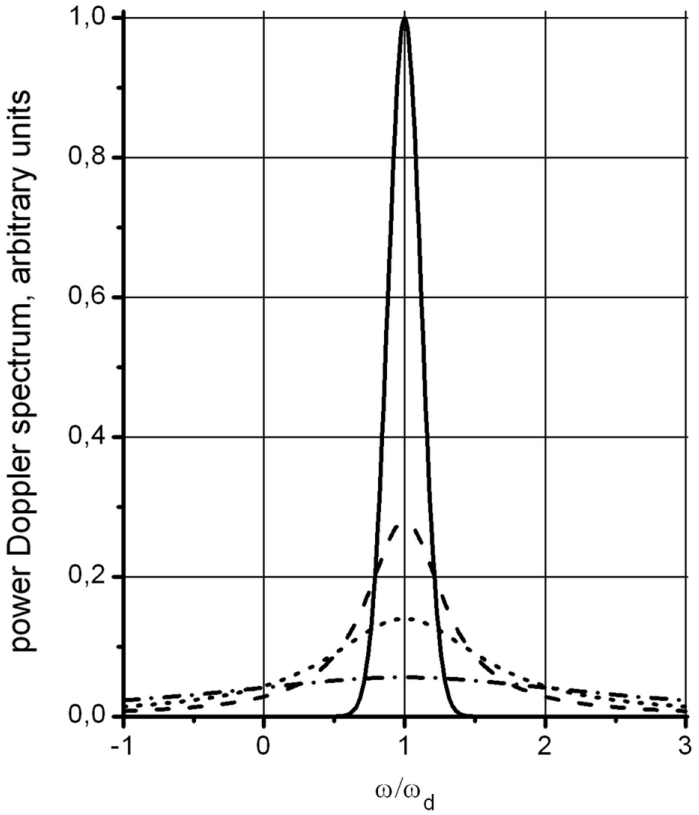

Figure 4. Power Doppler spectra for the nondiffusive case (solid line), and for diffusion with coefficients $D = 2D_{\mathrm{critical}}$ (dashed line), $D = 4D_{\mathrm{critical}}$ (dotted line), and $D = 10D_{\mathrm{critical}}$ (dash-dotted line).

The paper also derived an expression for the spectrum in the case of uniformly accelerated motion of inhomogeneities, which models blood flow in arteries:

$$S(\omega, y, z) = \lim_{T\to\infty} \nu k^4 \left\langle (\tilde{\beta} - \tilde{\rho})^2 \right\rangle T^{-1} \int \frac{dq_x}{2\pi} \, (q_x a)^{-1} \, |G(q_x + 2k\cos\vartheta, y, z)|^2 \, . \tag{15}$$

A distinctive feature of this result is that, in the limit of infinite observation time, the spectrum depends neither on frequency nor on the spatial characteristics of the probing field. Physically, this is because over a sufficiently long observation time all instantaneous velocities make equal contributions to the average signal power. Therefore, the frequency dependence caused by accelerated motion appears only for a finite observation time and depends on the initial phase of motion: the longer the acquisition interval, the broader the Doppler spectrum becomes (see Fig. 5).

On this basis, a model for vibrational sonoelastography was constructed in the paper. It was shown that the integrated power of the high-frequency part of the Doppler spectrum increases with increasing amplitude of the forced displacements, while changing the integration threshold makes it possible to enhance the contribution of regions with different oscillation amplitudes. This provides a physical basis for differentiating soft tissues by their mechanical stiffness. At the same time, the authors specifically noted that the power of the Doppler signal depends not only on the displacement amplitude, but also on fluctuations of density and compressibility; therefore, direct estimation of displacement requires additional compensation using the B-scan image.

Thus, [41] showed that even in the case of a stationary probing field, the Doppler spectrum is a complex characteristic determined jointly by the spatiotemporal properties of the scattering inhomogeneities and by the parameters of the ultrasound system. Within this model, steady blood flow, correlated motion, diffusion, harmonic vibrations, vibrational sonoelastography, and accelerated motion were described in a consistent manner. For this reason, this work is central to the further development of the entire topic: it established a general physical framework in which the Doppler response spectrum is viewed as the result of the interaction between the "physics of the medium" and the "physics of the measurement."

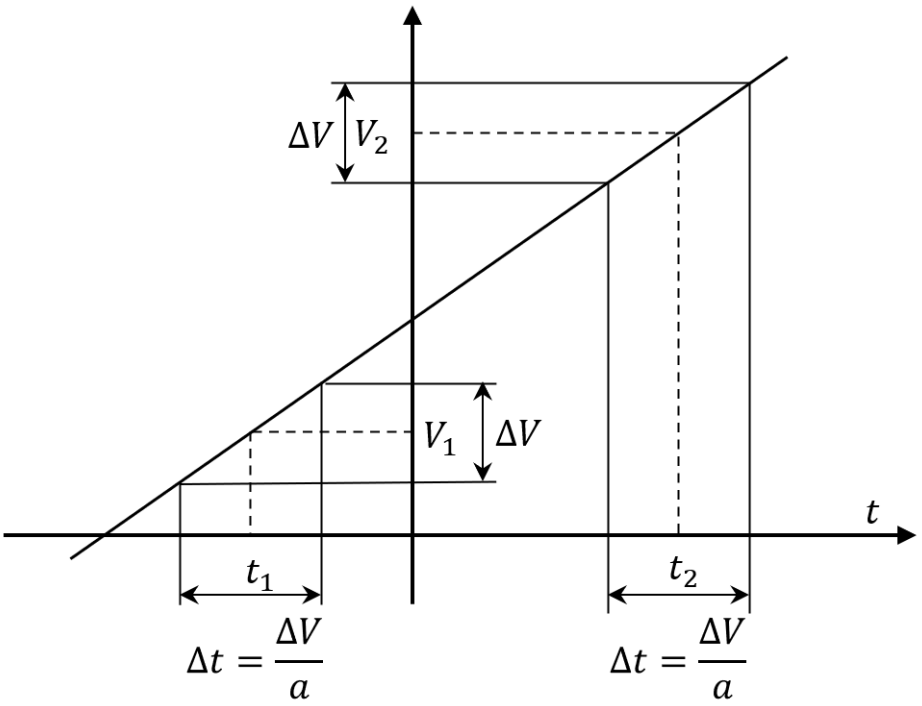

Figure 5. Velocity variation with time for uniformly accelerated motion. Equal velocity intervals ΔV correspond to equal time intervals Δt for all velocity values.

4. SPECTRA IN THE CASE OF DYNAMIC FOCUSING

The traditional approach described in the previous section has several limitations associated with focusing only at a fixed depth, an insufficient amount of data for accurate estimation of flow velocities, and limited spatial resolution. Therefore, in the subsequent studies, expressions for the spectra were obtained that generalize the case of a stationary probing field to the case of dynamic focusing. In principle, there are two possible ways to form the ultrasound Doppler signal using responses recorded for different angles of wave-vector rotation. In the first case, the signal is formed as a sequence of discrete responses corresponding to different successive insonification angles. Then, the power spectrum is determined not only by the spectral characteristics of the motion of the scattering inhomogeneities, but also by the spatial and temporal harmonics of the probing field itself [42]:

$$S(\omega_p) = \frac{k^4}{(2\pi)^3} \sum_{j=-\infty}^{\infty} \int d\vec{q}\, C(\vec{q}, \omega_p - \omega_j) \left| G(\vec{q} + 2\vec{k}, \omega_j) \right|^2, \tag{16}$$

where $\omega_p = 2\pi p/T$ is the Fourier-series variable, and T is the repetition period of signal acquisition for a given range of steering angles.

After the Doppler information has been extracted, the resulting complex signal values can be coherently summed for each point in space in order to provide dynamic focusing on transmission. This result establishes the general physical basis for all subsequent works on dynamic focusing.

Another method of forming the ultrasound Doppler signal, considered in [43], consists in the coherent summation of discrete responses obtained at different steering angles over the full period of angle variation T. This is equivalent to averaging the sensitivity function over the full insonification cycle. Such an approach requires a larger amount of computation, but it provides dynamic focusing during transmission. As a result, only the zero temporal harmonic of the sensitivity function remains in the expression for the spectrum, and the spectrum takes the form:

$$S(\omega_p) = T^2 \frac{k^4}{(2\pi)^3} \int d\vec{q}\, C(\vec{q}, \omega_p) \left| G(\vec{q} + 2\vec{k}, 0) \right|^2. \tag{17}$$

The authors emphasize that, in contrast to the first method, there is no frequency convolution here between the fluctuation correlator and the temporal harmonics of the sensitivity function. This means that the additional spectral broadening associated with the temporal variation of the insonification angle is substantially reduced. In this sense, the obtained expression is structurally similar to the formula for a stationary probing field, but unlike the traditional case, the advantages of synthetic aperture are preserved here, most notably high spatial resolution over a wide depth range.

Thus, coherent compounding makes it possible to combine improved transmit focusing with the absence of significant degradation in the spectral characteristics of the Doppler signal.

In [45], both methods of Doppler signal formation within plane-wave compounding were analyzed in more detail on the basis of a simple Gaussian model of the sensitivity function. In order to reduce the influence of the rectangular-window spectrum on the calculated spectrum, the authors used a Gaussian window T_W to obtain the following expression for the fluctuation correlator spectrum:

$$C(\vec{r}_1 - \vec{r}_0, \tau) = \nu \left\langle (\tilde{\beta} - \tilde{\rho})^2 \right\rangle \delta(\vec{r}_1 - \vec{r}_0 - \tau\vec{V}). \tag{18}$$

The sensitivity function was treated in the same framework. This made it possible to obtain smoothed expressions both for the fluctuation correlator spectrum and for the spectrum of the sensitivity function, without the side lobes characteristic of rectangular apodization. For clarity, the authors considered an explicit sensitivity function which, with the above weighting window taken into account, acquired a Gaussian form and, for the cases of coherent accumulation of signals and of obtaining the signal directly from Doppler angular responses, was given, respectively, by

$$G(\vec{r}, \omega_j = 0) = T^{-1}\sqrt{\pi T_W^2}\exp\left(-\frac{2\vec{r}^{\,2}}{a^2}\right) \tag{19}$$

and

$$G(x, y, z, \omega_j) = T^{-1}\sqrt{\pi T_W^2}\,\exp\left(-\frac{T_W^2(k\Omega y' + \omega_j)^2}{4}\right)\exp\left(-\frac{x^2 + y^2 + 2z^2 + (x' - l_0)^2}{a^2}\right). \tag{20}$$

Accordingly, for coherent accumulation, the spectrum obtained with account of (19) takes the form

$$S(\omega_p) = \nu \left\langle (\tilde{\beta} - \tilde{\rho})^2 \right\rangle T^{-1}k^4\frac{\pi^3 a^3}{4}\sqrt{\frac{T_W^2 a^2}{a^2 + T_W^2 V^2}}\exp\left[-\frac{T_W^2 a^2}{a^2 + T_W^2 V^2}\,\frac{(\omega_p - \omega_d)^2}{4}\right]. \tag{21}$$

$$\sigma^2 = 2\frac{a^2 + T_W^2 V^2}{T_W^2 a^2} = 2\left(\frac{1}{T_W^2} + \frac{V^2}{a^2}\right). \tag{22}$$

Here, $\omega_d = -2kV\cos\vartheta$ is the Doppler frequency shift, and σ^2 is the variance of the Doppler spectrum.

Within this model, the spectrum for coherent accumulation of signals obtained at different wave-tilt angles is Gaussian, with a maximum at the classical Doppler frequency. Its width is determined by two physical factors: the duration of the weighting window T_W, which effectively limits the signal length, and the characteristic size a of the measurement volume. In this sense, even for synthetic aperture, coherent compounding does not introduce a fundamentally new mechanism of spectral broadening: the additional contribution to the variance is associated only with the finite signal duration, whereas the structure of the spectrum itself remains close to that of the stationary insonification case. For this reason, the paper concludes that coherent compounding makes it possible to preserve improved focusing and spatial resolution without significant deterioration of the spectral characteristics of the Doppler signal.

A different situation arises when the Doppler signal is formed directly from the sequence of responses recorded at different angles of wave-vector rotation, using the sensitivity function (20). In this case, the spectrum takes the form

$$S(\omega_p) = \left\langle (\tilde{\beta} - \tilde{\rho})^2 \right\rangle k^4 T^{-2} T_W^2\frac{\pi^2 a^4}{8}\sqrt{\frac{\pi}{2a^2 + T_W^2 V^2}}\exp\left[-\frac{T_W^2 a^2(\omega_p - \omega_d)^2}{4(2a^2 + T_W^2 V^2)}\right]. \tag{23}$$

and the variance is

$$\sigma^2 = 2\frac{2a^2 + T_W^2 V^2}{T_W^2 a^2} = 2\left(\frac{2}{T_W^2} + \frac{V^2}{a^2}\right). \tag{24}$$

In this case, the spectral variance is larger than that for coherent compounding, and the difference between them is given by the additional term $\Delta\sigma^2 = 2/T_W^2$. Thus, in comparison with coherent accumulation, an additional mechanism of spectral broadening appears here, one that is reduced neither to the size of the measurement volume nor to the duration of the signal itself. Physically, this effect is associated with the fact that when the wave tilt angle changes, the Doppler angle also changes, and hence so does the projection of the velocity of the inhomogeneity motion onto the direction of the current wave vector, as shown in Fig. 6.

The authors interpreted this situation as motion with an effective acceleration inversely proportional to the time T_W. They also showed that the sign of this effective "acceleration" does not affect the spectral width: both for increasing and decreasing apparent velocity projection, the range of instantaneous values remains the same, so the variance contains precisely the quadratic term $2/T_W^2$. This also leads to a practical conclusion: the larger the interval T_W, the smaller the rate

of change of the Doppler angle within one window, and hence the smaller the additional spectral broadening for a given angular range $\Phi_{\max}$ (Fig. 6). The authors state that such terms may be neglected when the strong inequality

$$\frac{1}{T_W^2} \ll \frac{V^2}{a^2}$$

is satisfied, which is well fulfilled in real ultrasound systems.

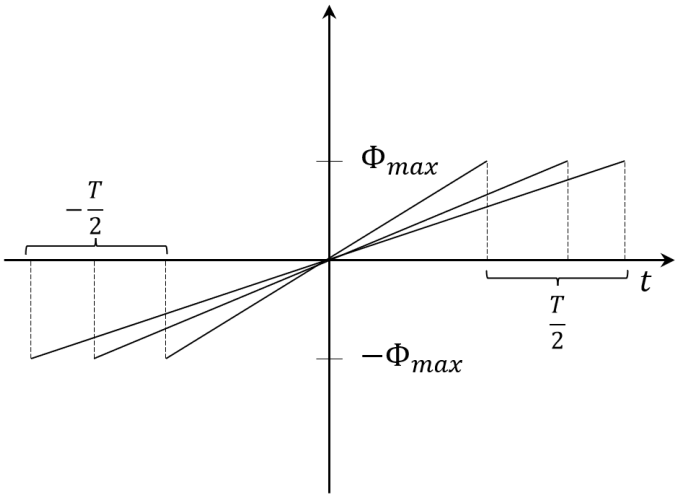

Figure 6. Model time dependence of the wave-vector deviation angle.

A separate part of the study considered the formation of compounding signals by cyclic permutation, where each new complex signal includes the contribution from a new insonification angle. For this method of constructing the sequence of compounding signals, the phase difference between neighboring samples does not accumulate additionally, unlike in the signal formed directly from individual angular responses. This means that the additional spectral broadening associated with variation of the Doppler angle is absent in this case (Fig. 7).

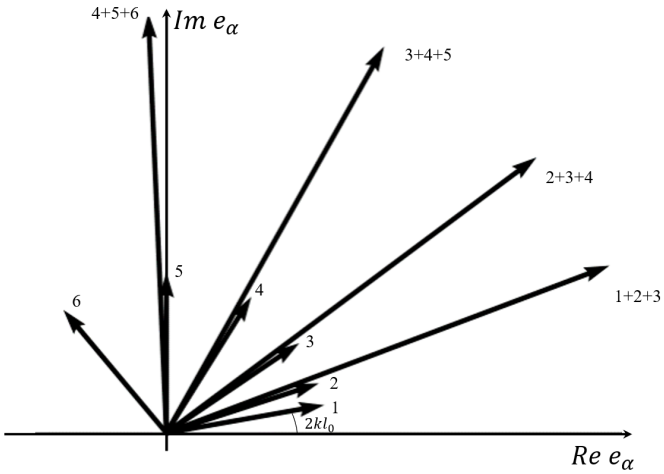

Figure 7. Nonlinear temporal growth of the phase difference $\Delta\varphi_n$ for the complex Doppler signal e_d and the phase difference for compounded signals e_c for the case of three steering angles, $N = 3$. Here, e_d^{ni} denotes the Doppler-response signal for the nth steering angle during the ith insonification period; the compounded signals are formed by cyclic permutation as successive sums such as $e_c^{11} + e_c^{21} + e_c^{31}$, $e_c^{21} + e_c^{31} + e_c^{12}$, $e_c^{31} + e_c^{12} + e_c^{22}$, $e_c^{12} + e_c^{22} + e_c^{32}$, and so on, with each new sum including the signal from the next insonification angle.

For this reason, cyclic permutation is an important practical way to preserve the accuracy of velocity estimation without losing time waiting for a complete set of signals from all steering angles.

Thus, in [45], it was shown that when plane-wave compounding is used, the width of the Doppler spectrum is determined not only by the parameters of the measurement volume and the signal duration, but also by the very method used to form the Doppler response. In coherent compounding, spectral broadening is caused mainly by the finite signal

duration, whereas forming the signal directly from the sequence of angular responses leads to additional broadening due to the dynamic change in the Doppler angle. This gives the effect a clear physical meaning and at the same time determines which processing method is more suitable for accurate Doppler measurements.

5. DIRECTIONS FOR FURTHER DEVELOPMENT OF THE TOPIC

Within the classical spectral formulation, the problem of forming the Doppler response in biological media has already been studied to a considerable extent. The previous sections considered stationary motion regimes, the influence of correlation and diffusion, nonstationary accelerated motion, oscillatory regimes and vibrational sonoelastography, as well as cases of dynamic variation of the insonification geometry and plane-wave compounding. In other words, within the framework of the traditional spectral model, the main physical scenarios determining the shape of the Doppler spectrum have already been described for both stationary and nonstationary motion regimes, as well as for modern insonification schemes with a dynamic sensitivity function.

A natural next step is the transition to shear-wave elastography, where the motion of the medium is no longer purely kinematic but has a wave character. In contemporary studies in this field, several approaches can be distinguished. Some works are devoted to recovering the shear-wave propagation velocity from the spatiotemporal characteristics of the wave field [47]. Another group of studies focuses on determining the complex shear modulus and the viscoelastic parameters of the medium on the basis of dispersion relations and spectral estimates [48, 49]. Separate developments address methods that take into account anisotropy and the tensor nature of the elastic properties of soft tissues [50], as well as general models of shear-wave propagation in viscoelastic media governed by different rheological laws [51]. More recent studies have proposed local-phase and wavenumber-based methods for estimating wave-process parameters, in particular the local phase-gradient approach [52] and local phase-velocity imaging using wavenumber filter banks [53].

At the same time, most existing approaches are aimed primarily at recovering the shear-wave velocity, its dispersive characteristics, or the complex shear modulus. In contrast, the problem of an analytical description of the fluctuation spectrum of the scattered ultrasound signal formed by shear-wave-induced displacement of the medium has not yet been formulated in a complete form. This is precisely the direction proposed for further research. It is proposed to use the eikonal of the shear wave, $\tau(\vec{r})$, as a linking quantity between the wave kinematics of the medium and the fluctuation spectrum of the Doppler response. If the local displacement is written in the form

$$u(\vec{r}, t) = A(\vec{r}) \exp\left[i(\omega t - \omega\tau(\vec{r}))\right], \tag{25}$$

then the function $\tau(\vec{r})$ defines the spatial phase distribution of the wave process and, consequently, the law governing modulation of the fluctuations of the scattering inhomogeneities. This opens the possibility of moving from an eikonal description of the shear-wave front to the construction of the fluctuation correlation function and, subsequently, to the Doppler signal spectrum. Thus, the further development of this line of research consists in establishing an analytical relation between the eikonal of the shear wave and the fluctuation spectrum of the scattered ultrasound response, which may potentially make it possible to relate the measured spectral characteristics of the signal to the local viscoelastic properties of the medium.

CONCLUSIONS

This paper summarizes physical approaches to describing the spectrum of the ultrasonic Doppler response in biological media on the basis of a continuous scattering model involving small fluctuations of density and compressibility. It is shown that, within this model, the spectral characteristics of the signal are determined by the combined action of two factors: the spatiotemporal structure of the medium fluctuations and the sensitivity function of the ultrasound system. On this basis, the cases of a stationary probing field were considered consistently for different regimes of inhomogeneity motion, including steady motion with constant velocity, motion with finite spatial correlation, diffusive mixing, uniformly accelerated motion, and harmonic oscillations. It was also shown how these regimes manifest themselves in the Doppler signal spectrum and in vibrational sonoelastography problems. It is emphasized separately that even in the classical case, the spectral shape is determined not only by the kinematics of the scatterers, but also by the geometry of the ultrasound field, the parameters of the measurement volume, and the character of spatial averaging.

Further development of the topic is associated with the transition to schemes with a dynamically varying sensitivity function, primarily dynamic focusing and plane-wave compounding. It is shown that in such systems the Doppler response spectrum depends not only on the motion of the inhomogeneities, but also on the very method of signal formation. For coherent plane-wave compounding, it was established that this approach makes it possible to combine improved focusing and high spatial selectivity without substantial additional spectral broadening, whereas forming the signal directly from the sequence of angular responses leads to additional spectral broadening due to the dynamic change of the Doppler angle. It was also shown that the spatial resolution in the plane-wave compounding mode is determined both by the interference properties of the set of angular responses and by the geometry of their overlap region, while its principal scales can be expressed through the parameters of the angular sector and the measurement volume. Thus, the present review covers the main stationary and nonstationary regimes of Doppler spectrum formation, modern methods of signal construction in plane-wave compounding, and the associated spatial-resolution properties of the system.

A promising direction for future work is the extension of this spectral theory to problems of shear-wave elastography by establishing an analytical relation between the eikonal of the shear wave and the fluctuation spectrum of the scattered ultrasonic signal.

ORCID

Evgen A. Barannik, https://orcid.org/0000-0002-3962-9960; **Mykhailo O. Hrytsenko**, https://orcid.org/0000-0002-5174-5542

REFERENCES

[1] D.G. Paeng, C.A. Lee, and C. Imtiaz, Principles of Doppler ultrasound and emerging blood flow imaging," Ultrasonography, **44**(6), 409–424 (2025). https://doi.org/10.14366/usg.25152

[2] N. Tsedendamba, Y. Song, E.-Y. Park, and J. Kim, "Review of Linear-Array-Transducer-Based Volumetric Ultrasound Imaging Techniques and Their Biomedical Applications," Bioengineering, **12**(9), 906 (2025). https://doi.org/10.3390/bioengineering12090906

[3] M.U. Aziz, J.R. Eisenbrey, A. Deganello, M. Zahid, K. Sharbidre, P. Sidhu, and M.L. Robbin, "Microvascular Flow Imaging: A State-of-the-Art Review of Clinical Use and Promise," Radiology, **305**(2), 250–264 (2022). https://doi.org/10.1148/radiol.213303

[4] R. Seddiki, T. Mirault, J. Sitruk, N. Mohamedi, E. Messas, M. Pernot, J. Baranger, and G. Goudot, "Advancements in Noncontrast Ultrasound Imaging for Low-Velocity Flow: A Technical Review and Clinical Applications in Vascular Medicine," Ultrasound in Medicine & Biology, **51**(7), 1035–1042 (2025). https://doi.org/10.1016/j.ultrasmedbio.2025.03.001

[5] J.Y. Gao, and C. Hou, "Progresses and clinical application of super-resolution ultrasound imaging: a narrative review," The Ultrasound Journal, **17**(1), 29 (2025). https://doi.org/10.1186/s13089-025-00432-6

[6] J.A. Jensen, S.I. Nikolov, K.L. Gammelmark, and M.H. Pedersen, "Synthetic aperture ultrasound imaging," Ultrasonics, **44**(Suppl. 1), e5–e15 (2006). https://doi.org/10.1016/j.ultras.2006.07.017

[7] G. Montaldo, M. Tanter, J. Bercoff, N. Benech, and M. Fink, "Coherent plane-wave compounding for very high frame rate ultrasonography and transient elastography," IEEE Transactions on Ultrasonics, Ferroelectrics, and Frequency Control, **56**(3), 489–506 (2009). https://doi.org/10.1109/TUFFC.2009.1067

[8] J. Viti, H.J. Vos, N. de Jong, F. Guidi, and P. Tortoli, "Detection of Contrast Agents: Plane Wave Versus Focused Transmission," IEEE Transactions on Ultrasonics, Ferroelectrics, and Frequency Control, **63**(2), 203–211 (2016). https://doi.org/10.1109/TUFFC.2015.2504546

[9] D. Jang, J. Park, J.H. Song, T.K. Song, and H. Yoon, "Investigation of ultrasound plane-wave imaging for optimal synthetic focusing," Scientific Reports, **16**(1), 1057 (2025). https://doi.org/10.1038/s41598-025-30595-0

[10] Y. Pan, X. Wang, Y. Qiang, N. Wang, R. Liu, G. Yang, Z. Zhang, X. He, Y. Yu, H. Zheng, and W. Qiu, "A New Method of Plane-Wave Ultrasound Imaging Based on Reverse Time Migration," IEEE Transactions on Biomedical Engineering, **71**(5), 1628–1639 (2024). https://doi.org/10.1109/TBME.2023.3346194

[11] L.C. Neves, F.M. Ribas, J.M. Maia, A.J. Zimbico, A.A. Assef, and E.T. Costa, "Improving Ultrasound B-Mode Image Quality with Coherent Plane-Wave Compounding Using Adaptive Beamformers Based on Minimum Variance," Sensors, **25**(5), 1306 (2025). https://doi.org/10.3390/s25051306

[12] S. Afrakhteh and L. Demi, "Coherent Plane Wave Compounding combined with Euclidean distance transform for high frame rate and high contrast ultrafast imaging," Ultrasonics, **156**, 107759 (2025). https://doi.org/10.1016/j.ultras.2025.107759

[13] J.S. Honer and R.J. McGough, "Fast and Accurate Plane Wave and Color Doppler Imaging with the FOCUS Software Package," Sensors, **25**(14), 4276 (2025). https://doi.org/10.3390/s25144276

[14] L. Basavarajappa, R. R, R. Tushar, and A.K. Thittai, "Toward Real-Time GPU Implementation of Diverging Beam With Synthetic Aperture Technique With Non-linear Beamforming for a Curvilinear Array," Ultrasound Imaging, (2025). https://doi.org/10.1177/01617346251406540

[15] B.A. Herrema, N.J. Eshkalak, and N. Bottenus, "Improved Spatiotemporal Resolution in Echocardiography Using Mixed Geometry Imaging Sequences," IEEE Transactions on Ultrasonics, Ferroelectrics, and Frequency Control, **71**(4), 438–447 (2024). https://doi.org/10.1109/TUFFC.2024.3364051

[16] C.-C. Shen and C.-L. Huang, "Improvement in Multi-Angle Plane Wave Image Quality Using Minimum Variance Beamforming with Adaptive Signal Coherence," Sensors, **24**(1), 262 (2024). https://doi.org/10.3390/s24010262

[17] Y. Xu, B. Li, J. Luo, X. Liu, and D. Ta, "Frame rate improvement in coherent plane-wave compounding using null subtraction imaging," AIP Advances, **14**(6), 065001 (2024). https://doi.org/10.1063/5.0201371

[18] J. Foiret, X. Cai, H. Bendjador, *et al.*, "Improving plane wave ultrasound imaging through real-time beamformation across multiple arrays," Scientific Reports, **12**, 13386 (2022). https://doi.org/10.1038/s41598-022-16961-2

[19] M. Hashemseresht, S. Afrakhteh, and H. Behnam, "High-resolution and high-contrast ultrafast ultrasound imaging using coherent plane wave adaptive compounding," Biomedical Signal Processing and Control, **73**, 103446 (2022). https://doi.org/10.1016/j.bspc.2021.103446

[20] S. Afrakhteh and H. Behnam, "Coherent Plane Wave Compounding Combined With Tensor Completion Applied for Ultrafast Imaging," IEEE Transactions on Ultrasonics, Ferroelectrics, and Frequency Control, **68**(10), 3094–3103 (2021). https://doi.org/10.1109/TUFFC.2021.3087504

[21] R. Paridar, and B.M. Asl, "Frame rate improvement in ultrafast coherent plane wave compounding," Ultrasonics, **135**, 107136 (2023). https://doi.org/10.1016/j.ultras.2023.107136

[22] C. Golfetto, I.K. Ekroll, H. Torp, L. Lovstakken, and J. Avdal, "Retrospective Transmit Beamforming and Coherent Plane-Wave Compounding for Microvascular Doppler Imaging: A Comparison Study," IEEE Transactions on Ultrasonics, Ferroelectrics, and Frequency Control, **68**(4), 1105–1116 (2021). https://doi.org/10.1109/TUFFC.2020.3033719

[23] C.-C. Shen, and Y.-C. Chu, "DMAS Beamforming with Complementary Subset Transmit for Ultrasound Coherence-Based Power Doppler Detection in Multi-Angle Plane-Wave Imaging," Sensors, **21**(14), 4856 (2021). https://doi.org/10.3390/s21144856

[24] X. Yan, Y. Qi, Y. Wang, and Y. Wang, "High Resolution, High Contrast Beamformer Using Minimum Variance and Plane Wave Nonlinear Compounding with Low Complexity," Sensors, **21**(2), 394 (2021). https://doi.org/10.3390/s21020394

[25] K. Miura, H. Shidara, T. Ishii, K. Ito, T. Aoki, Y. Saijo, and J. Ohmiya, "Image quality improvement in single plane-wave imaging using deep learning," Ultrasonics, **145**, 107479 (2025). https://doi.org/10.1016/j.ultras.2024.107479

[26] N. Chennakeshava, B. Luijten, O. Drori, M. Mischi, Y.C. Eldar, and R.J.G. van Sloun, "High Resolution Plane Wave Compounding Through Deep Proximal Learning," in: *2020 IEEE International Ultrasonics Symposium (IUS)* (2020). https://doi.org/10.1109/IUS46767.2020.9251399

[27] T. Miller, N. Chambara, M.T.C. Ying, and M.Y.C. Pang, "Using ultrafast angio planewave ultrasensitive and conventional doppler imaging techniques to assess intramuscular blood perfusion in older adults," BMC Medical Imaging, **24**(1), 324 (2024). https://doi.org/10.1186/s12880-024-01495-y

[28] K.L. Lai, M.C. Tsai, and P.C. Li, "Ultrafast Doppler Imaging for Early Detection of Synovitis in Rheumatoid Arthritis," Ultrasound in Medicine & Biology, **50**(4), 484–493 (2024). https://doi.org/10.1016/j.ultrasmedbio.2023.12.007

[29] G. Ivanac, A. Bulum, A.B. Jagnjić, *et al.*, "Advantages of Ultrafast ultrasound in the screening for renal artery disease," Journal of Ultrasonography, **24**(97), 1–6 (2024). https://doi.org/10.15557/jou.2024.0016

[30] M.B. Nguyen, N. Zhang, L.L. Mertens, *et al.*, "Noninvasive assessment of myocardial perfusion using ultrafast ultrasound: clinical study for congenital heart disease," European Heart Journal – Imaging Methods and Practice, **3**(1), qyaf007 (2025). https://doi.org/10.1093/ehjimp/qyaf007

[31] G. Ma, L. Chen, Y. Wang, *et al.*, "Application of microvascular ultrasound-assisted thyroid imaging report and data system in thyroid nodule risk stratification," Insights into Imaging, **15**(1), 230 (2024). https://doi.org/10.1186/s13244-024-01806-5

[32] J. Ji, E. Tang, Y. Wang, and X. Shi, "The Clinical Application of Superb Microvascular Imaging in Evaluating Thyroid Related Diseases: A Systematic Review," Journal of Clinical Ultrasound, **53**(2), 336–342 (2025). https://doi.org/10.1002/jcu.23863

[33] W. Li, Z. Ge, S. Cai, *et al.*, "Diagnostic value of greyscale ultrasound combined with superb microvascular imaging in thyroid nodules: a systematic review and meta-analysis," Quantitative Imaging in Medicine and Surgery, **15**(1), 440–454 (2025). https://doi.org/10.21037/qims-24-1195

[34] X. Hou, Z. Li, Y. Liu, J. Gao, and T. Song, "Diagnostic value of super-resolution ultrasound imaging in differentiating benign and malignant BI-RADS-4 breast lesions," Frontiers in Oncology, **15**, 1662492 (2025). https://doi.org/10.3389/fonc.2025.1662492

[35] S. Sabeti, N.B. Larson, J.C. Boughey, *et al.*, "Ultrasound-based quantitative microvasculature imaging for early prediction of response to neoadjuvant chemotherapy in patients with breast cancer," Breast Cancer Research, **27**(1), 24 (2025). https://doi.org/10.1186/s13058-025-01978-y

[36] Y. Zuo, Y. Zhan, J. Zhou, *et al.*, "Prediction of pathological complete response to neoadjuvant chemotherapy for invasive breast cancers based on longitudinal ultrasound and superb microvascular imaging: a single-center retrospective study," PeerJ, **13**, e20171 (2025). https://doi.org/10.7717/peerj.20171

[37] O. Tokur, S. Aydin, F. Kilinc, *et al.*, "Diagnostic value of super microvascular imaging in differentiating axillary lymph nodes: semi-quantitative and qualitative approach in primary breast cancer and suspicious axillary nodes," BMC Cancer, **25**(1), 1705 (2025). https://doi.org/10.1186/s12885-025-14936-w

[38] S. Xia, Q. Hua, Y. Song, *et al.*, "Super-resolution ultrasound imaging of intranodal lymphatic sinuses for predicting sentinel lymph node metastasis in breast cancer: a preliminary study," European Radiology, **35**(10), 6079–6088 (2025). https://doi.org/10.1007/s00330-025-11520-5

[39] E.A. Barannik, "Pulsed Doppler flow-line spectrum for focused transducers with apodized apertures," Ultrasonics, **39**(4), 311–317 (2001). https://doi.org/10.1016/S0041-624X(01)00059-2

[40] P.J. Fish, "Doppler methods," in: *Physical Principles of Medical Ultrasonics*, edited by C.R. Hill, (Ellis Horwood, Chichester, 1986), Chap. 11, pp. 338–376.

[41] E. Barannik, and I. Skresanova, "Correlation functions and power spectra of Doppler response signals in ultrasonic medical applications," Ultrasonics, **52**(5), 676–684 (2012). https://doi.org/10.1016/j.ultras.2012.01.014

[42] E.A. Barannik, and O.S. Matchenko, "The influence of the dynamic change of ultrasound system sensitivity function on the spectra of Doppler response signals," East European Journal of Physics, (2016). https://doi.org/10.26565/2312-4334-2016-2-08

[43] I.V. Sheina, O.B. Kiselov, and E.A. Barannik, "Power Spectra of Doppler Response Signals from Biological Objects Using Synthetic Aperture Ultrasound," East European Journal of Physics, **4**, 5–12 (2020). https://doi.org/10.26565/2312-4334-2020-4-01

[44] I.V. Sheina, and E.A. Barannik, "Resolution of the Ultrasound Doppler System Using Coherent Plane-Wave Compounding Technique," East European Journal of Physics, **1**, 116–122 (2022). https://doi.org/10.26565/2312-4334-2022-1-16

[45] E.A. Barannik, and M.O. Hrytsenko, "Spectra of Ultrasound Doppler Response Using Plane-Wave Compounding Technique," East European Journal of Physics, **1**, 476–484 (2024). https://doi.org/10.26565/2312-4334-2024-1-52

[46] E.A. Barannik, and M.O. Hrytsenko, "Ultrasound Doppler System's Resolution Using Coherent Plane-Wave Compounding Technique," East European Journal of Physics, **1**, 350–356 (2025). https://doi.org/10.26565/2312-4334-2025-1-43

[47] J. McLaughlin, D. Renzi, K. Parker, and Z. Wu, "Shear wave speed recovery using moving interference patterns obtained in sonoelastography experiments," The Journal of the Acoustical Society of America, **121**(4), 2438–2446 (2007). https://doi.org/10.1121/1.2534717

[48] S. Kazemirad, S. Bernard, S. Hybois, A. Tang, and G. Cloutier, "Ultrasound Shear Wave Viscoelastography: Model-Independent Quantification of the Complex Shear Modulus," IEEE Transactions on Ultrasonics, Ferroelectrics, and Frequency Control, **63**(9), 1399–1408 (2016). https://doi.org/10.1109/TUFFC.2016.2583785

[49] S. Cui, G. Cloutier, M.-H. Roy Cardinal, H. Savoji, and P. Maghoul, "Simultaneous viscoelastic characterization of soft tissues based on shear wave ultrasound dispersion and multi-scale wavelet cross-correlation analysis," Mechanical Systems and Signal Processing, **237**, 112890 (2025). https://doi.org/10.1016/j.ymssp.2025.112890

[50] M. Correia, T. Deffieux, S. Chatelin, J. Provost, M. Tanter, and M. Pernot, "3-D elastic tensor imaging in weakly transversely isotropic soft tissues," Physics in Medicine & Biology, **63**, 155005 (2018). https://doi.org/10.1088/1361-6560/aacfaf

[51] M. Osika, and P. Kijanka, "Ultrasound Shear Wave Propagation Modeling in General Tissue-Like Viscoelastic Materials," Ultrasound in Medicine & Biology, **50**(4), 627–638 (2024). https://doi.org/10.1016/j.ultrasmedbio.2024.01.008

[52] E. González-Mateo, F. Camarena, and N. Jiménez, *et al.*, "Real-time ultrasound shear wave elastography using a local phase-gradient method," Computer Methods and Programs in Biomedicine, (2025). https://doi.org/10.1016/j.cmpb.2024.108529

[53] R. Almasi, M.W. Urban, and P. Kijanka, "Local phase velocity imaging with wavenumber filter banks for ultrasound shear wave elastography," Computer Methods and Programs in Biomedicine, **269**, 108894 (2025). https://doi.org/10.1016/j.cmpb.2025.108894

ДОПЛЕРІВСЬКІ СПЕКТРИ ДЛЯ СТАЦІОНАРНИХ ТА ДИНАМІЧНИХ УЛЬТРАЗВУКОВИХ ПОЛІВ

Є.О. Баранник, М.О. Гриценко

Кафедра медичної фізики та біомедичних нанотехнологій, Харківський національний університет імені В. Н. Каразіна, майдан Свободи, 4, 61022, Харків, Україна

У цій роботі наведено огляд фізичних і методологічних підходів до опису спектра ультразвукового допплерівського сигналу в біологічних середовищах. Узагальнено результати щодо формування спектральних характеристик для стаціонарного зондувального поля за різних типів руху розсіювачів, а також розглянуто розвиток моделі для випадку динамічно змінної функції чутливості ультразвукової системи. Особливу увагу приділено режимам синтетичної апертури, динамічного фокусування та когерентного пласкохвильового компаундингу. Показано, що в системах пласкохвильової візуалізації спектр допплерівського сигналу визначається не лише властивостями руху середовища, а й просторово-часовим способом формування допплерівського відгуку. Також узагальнено результати щодо просторової роздільної здатності в режимі пласкохвильового компаундингу та проаналізовано зв'язок між геометрією вимірювального об'єму, функцією чутливості й спектральними параметрами. Окреслено перспективи подальшого розвитку цих підходів, зокрема для застосувань у зсувнохвильовій еластографії.

Ключові слова: *ультразвукова допплерівська візуалізація; допплерівський спектр; візуалізація із синтетичною апертурою; пласкохвильова візуалізація; когерентний пласкохвильовий компаундинг; просторова роздільна здатність; зсувнохвильова еластографія*